Journal of Experimental Marine Biology and Ecology 459 (2014) 51–60

Contents lists available at ScienceDirect

Journal of Experimental Marine Biology and Ecology

journal homepage: www.elsevier.com/locate/jembe

Distributions of invertebrate larvae and phytoplankton in a coastal upwelling system retention zone and peripheral front

J.P. Ryan [a,*], J.B.J. Harvey [a], Y. Zhang [a], C.B. Woodson [b]

[a] Monterey Bay Aquarium Research Institute, Moss Landing, CA 95039, USA
[b] COBIA Lab, College of Engineering, University of Georgia Athens, GA 30602, USA

ARTICLE INFO

Article history:
Received 1 February 2014
Received in revised form 18 May 2014
Accepted 19 May 2014
Available online xxxx

Keywords:
Coastal upwelling
Frontal dynamics
Larval ecology
Phytoplankton ecology
Autonomous underwater vehicles

ABSTRACT

Near-coastal retention of larvae affects the ecology of many marine species. In coastal upwelling ecosystems having strong offshore transport, larval ecology is greatly influenced by nearshore retention in bays and in the lee of headlands. Further, frontal dynamics along the periphery of retention zones can drive larval accumulation and transport. The purpose of this study is to examine larval distributions and associated processes across a retention zone and its peripheral front in the coastal upwelling environment of Monterey Bay, California, USA. During fall 2009 an autonomous underwater vehicle (AUV) was used to observe environmental variability at high resolution and acquire targeted water samples. Invertebrate larvae in samples were subsequently identified and quantified using molecular methods. To infer ecological processes we examine larval distributions in relation to environmental processes revealed by the AUV data and the greater regional observing system. As a window into biological–physical interactions that may concentrate motile larvae in convergence zones, we examine more extensive in situ and remote sensing observations that describe distribution patterns of motile phytoplankton. During the 10-day study intensification of upwelling caused flow of cold water into the bay and formation of an upwelling front. Drifter and satellite observations showed retention of near-surface water within the bay inshore of the front, where a bloom of motile phytoplankton intensified. Larval distributions were related to processes inferred at a range of scales. At the scale of the retention zone, dense phytoplankton accumulations indicated concentration of motile plankton in a convergence zone created by flow toward the coast, as well as nutritional support for larvae. At the scale of the front, velocity and water property measurements indicated convergence between cold deep-shelf water transported shoreward along shoaling bathymetry and the overlying warm surface water, influencing plankton accumulation and vertical transport. At the finest scales resolved, aerial photography revealed banded accumulations of dense phytoplankton bloom patches and narrow foam lines, common indicators of small-scale convergence zones and consistent with internal wave processes. Exceptionally high larval concentrations were detected in samples from locations affected by frontal and internal wave dynamics. This study illustrates how autonomous feature recognition and targeted sampling with an AUV, applied within the greater context of multidisciplinary observation across regional to small scales, can advance plankton ecology research.

1. Introduction

As agents of population persistence and connectivity, larvae are essential to the structure and function of coastal marine ecosystems (Carson, 2010; Cowen et al., 2006; Mace and Morgan, 2006). Advancing the understanding of larval ecology is thus essential to effective ecosystem based management (Davoren et al., 2007; Sponaugle, 2009). Only through understanding processes of larval ecology – and the associated forcing, scales, and interactions – can we design marine reserves to effectively sustain the biodiversity and resilience of marine communities (Fenberg et al., 2012; Gaines et al., 2010; Palumbi, 2003). However, difficult research challenges are presented by the small size of larvae relative to the scales of ocean dynamics, as well as the inherent complexity, patchiness and variability of both coastal marine ecosystems and larval populations. These challenges hinder our ability to understand the survival and transport of larvae and the cascading effects on ecosystems. This study presents results from novel methods designed to overcome some of these challenges. These methods integrate high-resolution multidisciplinary sensing and adaptively targeted sampling conducted simultaneously by an autonomous underwater vehicle (AUV), providing effective observation and sampling of plankton patchiness and its ecological context.

The study region, Monterey Bay (Fig. 1), resides in the dynamic California Current upwelling system. In coastal upwelling systems, an immense supply of nutrients to the photic zone supports tremendous productivity – from phytoplankton through zooplankton, fish, mammals

* Corresponding author. Tel.: +1 831 775 1978 (voice); fax: +1 831 775 1620.
E-mail addresses: ryjo@mbari.org (J.P. Ryan), Jharvey@mbari.org (J.B.J. Harvey), yzhang@mbari.org (Y. Zhang), bwoodson@uga.edu (C.B. Woodson).

http://dx.doi.org/10.1016/j.jembe.2014.05.017
0022-0981/

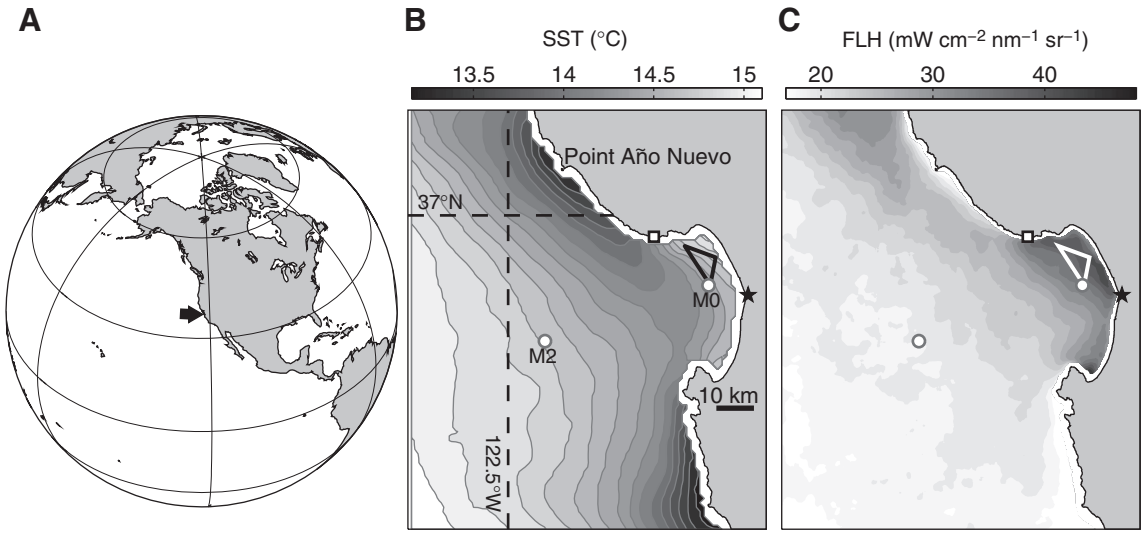

Fig. 1. Environmental setting and study design. (A) Geographic position of the study region along the northeastern Pacific margin. Fall climatological averages of (B) sea surface temperature (SST) and (C) chlorophyll fluorescence line height (FLH) from the MODIS Aqua satellite sensor are based on data from 2004 to 2008. The triangle over northern Monterey Bay represents the surface track of repeated AUV surveys conducted between 29 September and 8 October 2009. Moorings M0 and M2 provided continuous hourly measurements during the study (Figs. 2, 7). The star and square symbols indicate the locations for which predicted tidal height and zonal wind data, respectively, are examined relative to variation in water column conditions and circulation (Section 3.4).

and birds (Barber and Smith, 1981). While high primary productivity enhances larval food supply, strong offshore transport of surface water that drives coastal upwelling threatens larvae that must remain near shore for successful recruitment to adult habitats. In this context, bays and areas in the lee of coastal headlands, described as retention centers or upwelling shadows, are crucial (Graham et al., 1992; Morgan et al., 2011; Roughan et al., 2005).

Northern Monterey Bay contains a large retentive upwelling shadow (Graham et al., 1992). Physical distinction of this feature is evident as the warmest long-term averaged sea surface temperature (SST, Fig. 1B), while biological distinction at the level of phytoplankton is evident in the corresponding average of chlorophyll fluorescence (Fig. 1C). The spatial patterns of these distinctions represent regional atmospheric and oceanic circulation patterns, as shaped by coastal geomorphology (Breaker and Broenkow, 1994; Graham and Largier, 1997; Rosenfeld et al., 1994). Upwelled water typically approaches the bay as an along-coast flow from the north, originating around Point Año Nuevo (Fig. 1B). Eastward turning of the coastline at the northern end of the bay results in separation of upwelling flow from the coast, and a cyclonic gyre typically forms in the northern bay. The Santa Cruz Mountains along the bay's northern coast buffer northwesterly wind stress, thereby reducing wind-forced vertical mixing and enabling stratification. These geomorphological influences locally enhance residence time and thermal stratification in the upwelling shadow. Elevated chlorophyll concentrations in the upwelling shadow (Fig. 1C) reflect the blooming of phytoplankton within the relatively warm and stratified environment into which nutrients are episodically transported (Ryan et al., 2008, 2009, 2011). These conditions lead to comparatively great abundance and diversity of zooplankton within the upwelling shadow, the biological attribute essential to original distinction of the upwelling shadow as an ecological phenomenon (Graham et al., 1992).

The significance of retention centers and their peripheral fronts to larval ecology off northern California has been studied. Larval settlement and recruitment are greater in the sheltered lee of coastal headlands south of Point Reyes and Bodega Head than along the exposed coastline at Bodega Head (Mace and Morgan, 2006; Wing et al., 2003). Larvae of multiple taxa in all stages of development can be entrained and accumulated in a recirculation feature in the lee of Bodega Head (Morgan et al., 2011). Accumulation within retention zones during upwelling has been hypothesized as a mechanism of larval supply to more exposed and recruitment-limited sites when regional wind relaxation causes poleward transport around the coastal headland of the retention zone (Mace and Morgan, 2006; Wing et al., 2003). Integration of satellite remote sensing and in situ measurements of larval recruitment off California reveal that coastal upwelling fronts, including those that form along the periphery of retention centers, organize recruitment patterns of both community-building invertebrates in intertidal habitats and fishes in nearshore rocky reef habitats (Woodson et al., 2012). Hypothesized mechanisms include convergent flow at the front, which can drive accumulation of swimming larvae, and along-front transport toward the coast, which can funnel larvae to nearshore recruitment sites (Woodson et al., 2009). While these mechanisms have a sound theoretical basis, larval accumulation in the Monterey Bay upwelling shadow front has not been observed directly.

The importance of retentive zones and fronts to larval ecology motivates development and application of better methods to observe processes and sample populations. In this study we employ an AUV developed to respond to feature recognition based on real-time analysis of environmental data, and to acquire precisely located water samples. Larvae in samples are identified and quantified by molecular methods. These high-resolution observations are placed in a regional ecological context with multidisciplinary observations of a greater ocean observing system, to infer processes of importance to larval ecology. Our objectives are to describe ecological processes across horizontal scales of ~10^2 to 10^4 meters and to relate observed distributions of invertebrate larvae and phytoplankton to these processes.

2. Materials and methods

2.1. AUV surveys

The primary platform for observation and sampling was the *Dorado* AUV. *Dorado* has been applied to study a variety of complex coastal ocean processes in the Monterey Bay region, including zooplankton ecology (Harvey et al., 2012; Ryan et al., 2010a), phytoplankton ecology (Ryan et al., 2008, 2010b, 2014), upwelling dynamics (Fitzwater et al., 2003; Ryan et al., 2011), nutrient-based primary productivity rates (Johnson and Needoba, 2008), frontal processes (Ryan et al., 2010c), and internal wave dynamics (Cazenave et al., 2011). Toward effective plankton ecology research, the focus of the present study, the *Dorado* AUV provides key enabling capabilities: (1) a multidisciplinary sensor suite for measuring physical, chemical and optical properties, (2) fast

propulsion that supports synoptic observation in rapidly changing environments, (3) a rapid-intake water sampling system that permits acquisition of highly localized samples while the vehicle moves at high speed, and (4) autonomous algorithms that target water sample acquisition on ecological features of interest (Section 2.2).

Because of the importance of observing water column structure and variability in coastal marine ecology research, the AUV missions utilize a depth oscillation behavior while transiting between geographic waypoints, resulting in a 'sawtooth' sampling trajectory throughout the water column. The top of the depth envelope is fixed at 2 m and detected by measurement of pressure. The bottom of the depth envelope is variable and determined by acoustic detection of the bottom; in this study the AUV maintained a minimum altitude of ~7 m above bottom. Geographic position is determined by integrating data from periodic surfacing for GPS acquisition and Doppler-aided velocity estimates while the vehicle is underwater. Further details of the *Dorado* AUV, its sensors, and its water-sampling system are available in prior publications (Bellingham et al., 2000; Bird et al., 2007).

Design of the AUV survey track for this experiment was based on climatological patterns of SST and chlorophyll fluorescence from the Moderate Resolution Imaging Spectroradiometer (MODIS) Aqua satellite sensor (Fig. 1). Previous analyses have shown that fluorescence line height (FLH) from MODIS is more effective at describing intense blooms (Ryan et al., 2009), and the patterns of these blooms of motile phytoplankton are relevant to zooplankton ecological research, thus we used FLH instead of band-ratio chlorophyll estimates. The processing methods for the MODIS data are published (Ryan et al., 2009). The triangular AUV survey track (Fig. 1) was planned to achieve two goals: (1) sample different water types (recently upwelled, upwelling shadow, and the front between them), and (2) provide high-frequency repeat coverage in order to observe frontal dynamics. Frontal observations were anticipated to be most effective along the southeastern transect of the triangular AUV track, running approximately perpendicular to the mean front (Fig. 1B). Between 29 September and 8 October 2009, the AUV surveyed a distance of ~317 km in 12 partial to full iterations of the triangular track and acquired 36 water samples along with high-resolution ecological context from a multidisciplinary sensor suite.

To examine physical and biological patterns in the AUV observations, we present data from two sensors. The first is a Sea-Bird Electronics conductivity, temperature, depth (CTD) with SBE3 temperature sensor, SBE4 conductivity sensor, and SBE25 board set. Due to fouling of the CTD conductivity cell, caused by organic matter from abundant gelatinous zooplankton, salinity data were problematic and thus not used. The second is a HOBI Labs HS-2 sensor that measured chlorophyll fluorescence at 700 nm and optical backscattering at 420 and 700 nm wavelengths; data from this sensor were the basis for autonomously targeting water sampling.

2.2. AUV targeted water sampling

The *Dorado* AUV supports autonomously targeted whole water sampling of features identified by real-time analysis of sensor data. The algorithms used for feature identification are modular and adaptable. In the present study, algorithms developed for sampling within and outside of phytoplankton patches were deployed. The primary algorithm integrates multiple capabilities (Zhang et al., 2010, 2012). By targeting sampling at coincident peaks in fluorometric chlorophyll and optical backscattering, the algorithm ensures that subsurface peaks in chlorophyll fluorescence are true biomass maxima and not due to quenching of fluorescence near the surface (Cullen and Eppley, 1981; Holm-Hansen et al., 2000). By accumulating statistics of optical data within a temporal window, the algorithm adapts its sensitivity to ambient conditions. By enforcing minimum temporal separation between samples, the algorithm allocates sampling capacity within a survey. Most (72%) of the samples were acquired using the primary algorithm. The secondary algorithm was a simpler predecessor that controlled triggering of sample acquisition according to a predefined threshold in fluorometric chlorophyll values. It was used for comparative purposes because this experiment was the first in which the primary algorithm was being applied.

2.3. Larval identification and quantification

We used the sandwich hybridization assay (SHA), a detection system that quantifies target organism RNA molecules, to identify and assess relative abundances of mussel and barnacle larvae from AUV water samples (Goffredi et al., 2006; Harvey et al., 2013; Jones et al., 2008). Details of AUV Gulper water sample filtration, preservation and analysis by SHA are reported elsewhere (Goffredi et al., 2006; Jones et al., 2008; Ryan et al., 2010a). Numbers of invertebrate larvae per liter were estimated from SHA optical absorbance measurements ($\lambda = 450$ nm), which were calibrated using SHA dosage response curves reported by Goffredi et al. (2006) for *Balanus glandula*, and by Jones et al. (2008) for *Mytilus edulis*.

2.4. Regional ecological context

Regional ecological context was derived from remote sensing and in situ data. Two forms of satellite remote sensing data were used to examine the evolution of regional conditions during the study. The first was SST from the Advanced Very High Resolution Radiometer (AVHRR), which offers better temporal resolution than MODIS. AVHRR processing methods are documented (Ryan et al., 2010c). The second was full-resolution (300 × 300 m) Maximum Chlorophyll Index (MCI) images from the Medium Resolution Imaging Spectrometer (MERIS). The MCI quantifies the height of a near-infrared spectral peak caused by dense near-surface accumulations of motile phytoplankton (Gower et al., 2005). MCI has been used for studies of phytoplankton ecology in Monterey Bay and is an effective indicator of regions where convergent circulation results in the accumulation of motile dinoflagellates (Ryan et al., 2008, 2009, 2014). In this study, MCI images provided information on the patterns of physical–biological coupling that may cause accumulation of larvae and other swimming zooplankton. To examine small-scale patterns of phytoplankton accumulation, we used photographic observations of the study area acquired from an altitude of ~300 m on 6 October 2009.

Two moorings provided data for regional environmental context (Fig. 1B). Winds at mooring M2, ~25 km seaward of the bay mouth, represent regional wind forcing to which the upwelling centers north and south of Monterey Bay respond. Wind measurements were acquired using a R. M. Young wind monitor, model 05103. Water property and velocity measurements at mooring M0 describe hydrographic and circulation variability at the southern vertex of the AUV track (Fig. 1B). Considering the cyclonic circulation that typically develops within the bay during upwelling, data collected at M0 effectively describe the influence of upwelled waters entering the upwelling shadow. Water property measurements were acquired using Sea-Bird MicroCAT CTD sensors. A drifter designed to describe near-surface circulation (Manning et al., 2009) was deployed at the northeastern vertex of the AUV survey track during the period of peak upwelling response. The drifter's drogue was 1 m tall and was tethered 1 m below the surface.

3. Results and discussion

3.1. Environmental conditions

The study period was dominated by regional responses to upwelling. Transition from weak poleward winds to stronger equatorward (upwelling favorable) winds preceded the start of AUV surveys (Fig. 2A). Decreasing temperature and increasing salinity at mooring M0 defined the influence of upwelled water on the study domain, and most of the AUV observations occurred when the local anomalies of

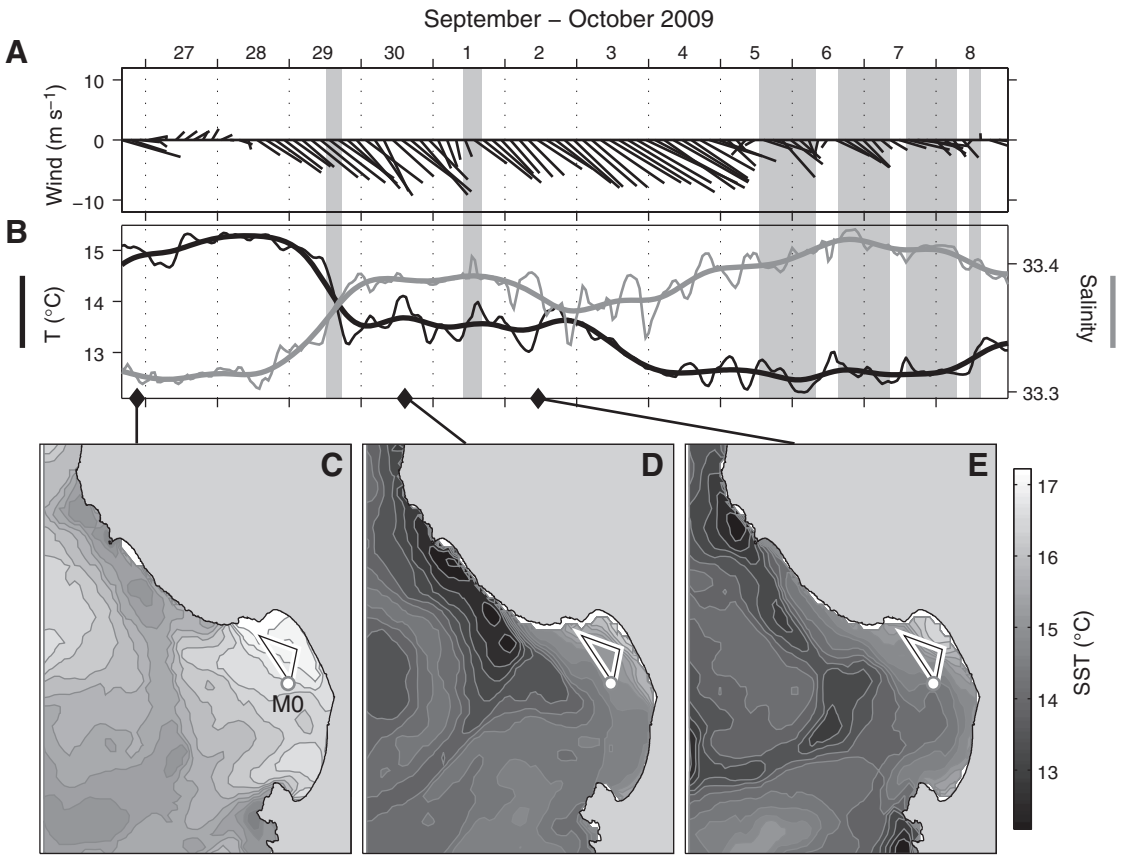

Fig. 2. Environmental conditions during the experiment. (A) Surface winds at mooring M2 (location shown in Fig. 1), representing regional wind forcing. Wind speed and direction are represented by the length and orientation of the vectors, respectively (vectors point in the direction of the wind). (B) Surface temperature and salinity at mooring M0 (location shown in Fig. 2C–E) are shown as hourly (thin lines) and 33-hour low-pass filtered (thick lines). Shading in (A, B) indicates AUV survey periods. (C–E) AVHRR sea surface temperature (SST) images; image acquisition times are indicated by black diamonds on the time axis of the M0 record (B).

upwelled water (cold, salty) were greatest (Figs. 2B, 5–8 October). The temporal lag between upwelling wind forcing (Fig. 2A) and hydrographic conditions of upwelling response at M0 (Fig. 2B) was due to advection from the upwelling center at Point Año Nuevo. Satellite SST images show advection patterns and reveal the regional consequences of upwelling (Fig. 2C–E). During the period of weak winds, 26–28 September, the bay was relatively warm and contained weak SST gradients (Fig. 2A–C). Following transition to stronger and upwelling-favorable winds, cold water that originated in the Point Año Nuevo upwelling center flowed into the bay. Resulting enhancement of thermal gradients at the upwelling shadow front was evident within the AUV survey domain (Fig. 2C–E).

SST in the study region was not clearly visible to satellite remote sensing during 3–8 October, precluding description of regional patterns. However, in situ observations show persistence of the upwelling anomalies and front. Cold, salty conditions intensified at M0 during 3–6 October (Fig. 2B). Although these anomalies weakened during 7–8 October, apparently as a lagged response to weakening of upwelling favorable winds beginning on 5 October, they nonetheless remained anomalous (cool, salty) relative to conditions at the start of the study

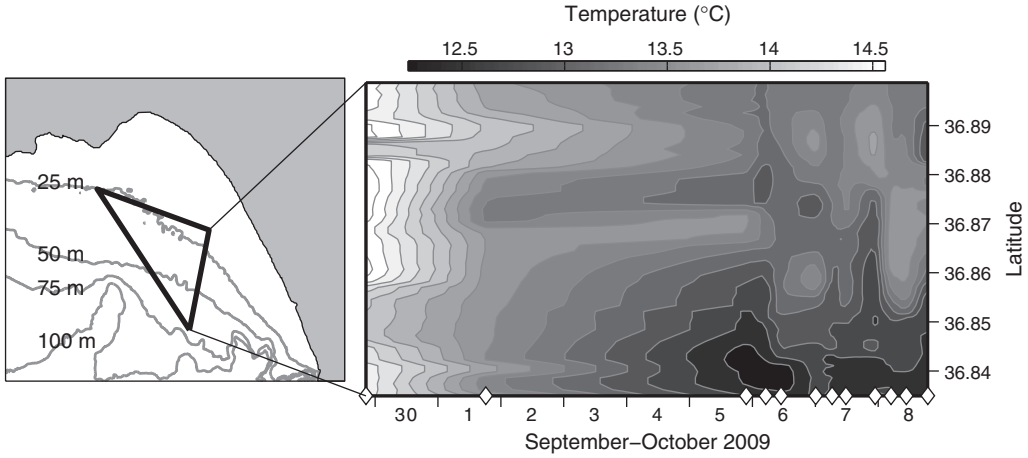

Fig. 3. Hovmoller plot of near-surface (averaged 3–5 m depth) temperature for the southeastern AUV transect. Diamonds on the time axis indicate the start time of each AUV transect.

(Fig. 2A,B). The southeastern AUV transect was oriented cross-shelf in the region where satellite SST showed the strongest front on 2 October (Fig. 2E). This transect was also most consistently sampled throughout the AUV time series. Near-surface temperature along this transect showed the development of the upwelling front, its persistence through the end of the study, and intensification of its gradients at the end of the study, 7–8 October (Fig. 3).

3.2. Overview of invertebrate larval abundance data

Larval abundance data are represented in temporal, spatial and ecological contexts in Fig. 4. Mussel and barnacle larvae were detected in AUV-acquired water samples throughout the time-series. Larval concentrations ranged between 0 and 90 L^{-1} (Fig. 4A). The highest larval concentrations were sampled late in the study period (Fig. 4A), when hydrographic anomalies of upwelling persisted at M0 (Fig. 2B) and frontal gradients were strongest (Fig. 3). Although the AUV could have sampled anywhere along the triangular survey track, most of the samples (89%) were acquired along the southeastern transect (Fig. 4B). This resulted from the application of autonomous sampling algorithms designed to target patches of high phytoplankton abundance (Section 2.2) and the presence of an intense phytoplankton bloom intersected by the southeastern transect (Section 3.3). Samples were acquired across a large range of chlorophyll concentrations and temperature (Fig. 4C). At a given temperature, higher larval abundances were typically detected in water having higher chlorophyll concentrations; this is emphasized for the two highest larval abundances detected (Fig. 4C). In Sections 3.4 and 3.5, we examine the full time-series along the southeastern AUV transect to illustrate processes and explore how physical processes related to exceptionally high larval abundances.

3.3. Influences and inferences from a dense phytoplankton bloom

Immediately prior to the start of AUV observations, a phytoplankton bloom was concentrated near the coast east of the AUV survey domain (Fig. 5A). Following the upwelling pulse (Fig. 2) the bloom increased in intensity and spatial scale (Fig. 5B, C). Phytoplankton-enriched filaments that extended across the AUV survey track suggest transport of near-coastal plankton into the AUV survey domain (Fig. 5B, C). Drifter observations of near-surface transport revealed approximately diurnal flow oscillations between inner shelf water, where the bloom was detected by remote sensing during the day, and the eastern region of the AUV survey (Fig. 5C). Drifter movement was consistent with retention of near-surface plankton within the upwelling shadow. AUV observation and sampling during 5–8 October occurred during most of each day (17–19 hours), increasing the potential to encounter advecting dense bloom patches (Fig. 5B, C).

In addition to influencing the spatial distribution of sampling (Section 3.2), the phytoplankton bloom provided ecological information relevant to understanding larval distributions. Studies of the Monterey Bay upwelling shadow show that exceptionally dense phytoplankton patches can identify where motile phytoplankton accumulate through biological-physical interactions (Ryan et al., 2008, 2009, 2014). Specifically, near-surface accumulation results from upward swimming of cells transported into convergence zones (Franks, 1997; Ryther, 1955; Stumpf et al., 2008). Thus, evidence of phytoplankton accumulation in

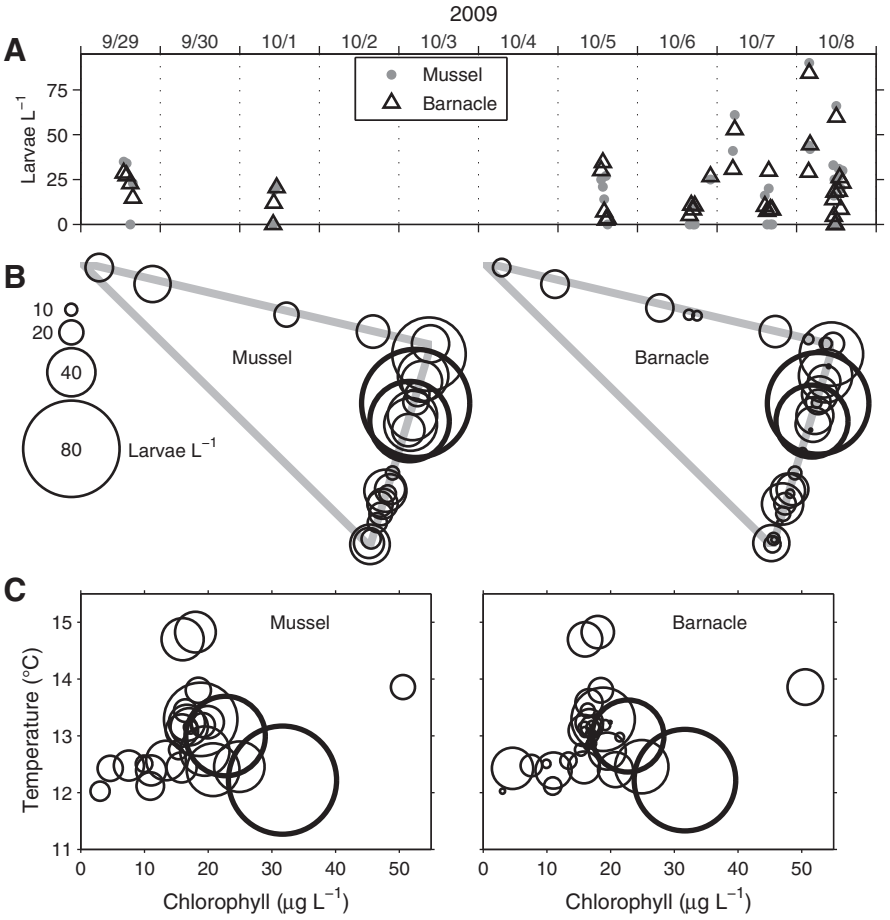

Fig. 4. Larval abundance results are represented in (A) temporal, (B) spatial and (C) ecological contexts. (A) Points on the bottom axis are samples in which no larvae were detected. The two highest concentrations of both barnacle and mussel larvae, detected in samples from sequential AUV transects 7 hours apart on 8 October (A), are indicated by the thick circles in (B, C).

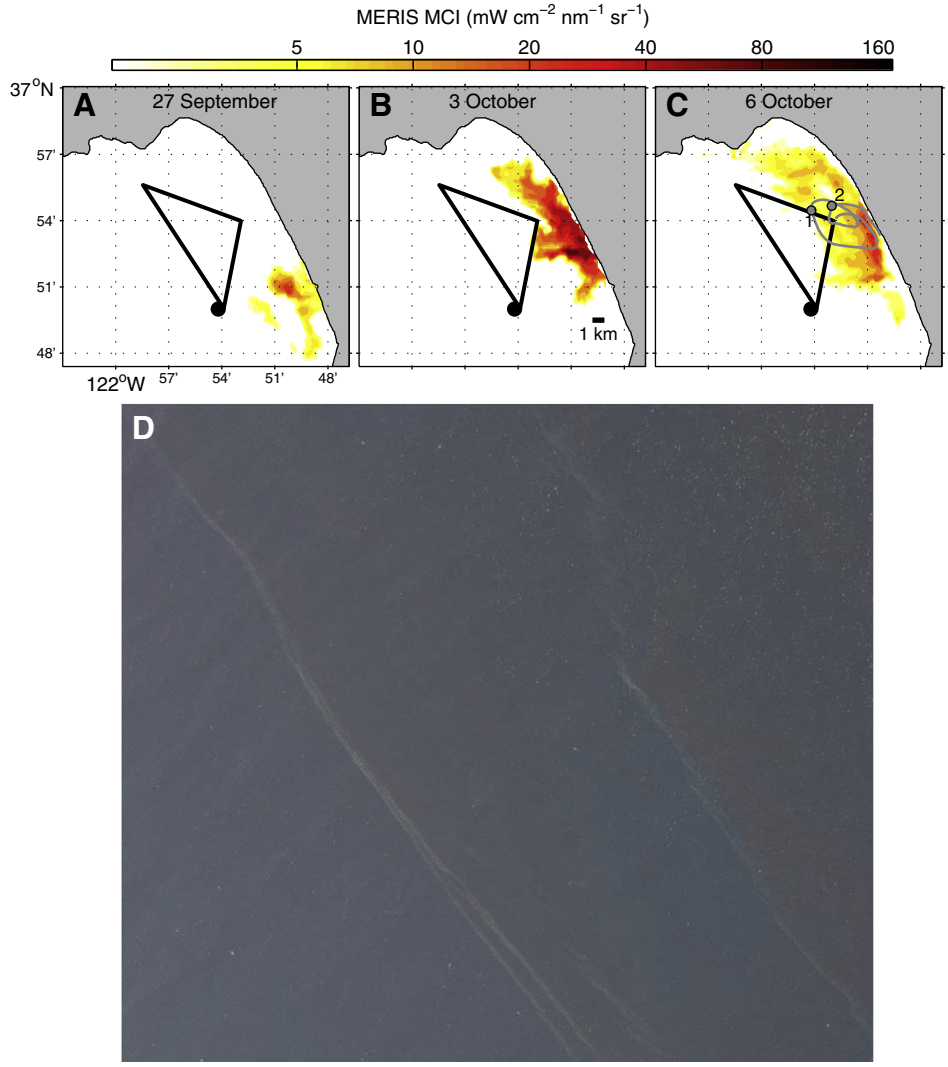

Fig. 5. Near-surface phytoplankton bloom patterns and circulation. (A–C) The MERIS MCI represents the near-infrared reflectance of dense surface accumulations of phytoplankton, in particular bloom-forming "red tide" dinoflagellates. The gray line in (C) shows near-surface (1–2 m depth) circulation patterns defined by a drifter released at the northeastern apex of the AUV survey track late on 5 October. The numbered points are 1 and 2 days after drifter release. (D) Aerial photograph of phytoplankton accumulations (banded reddish coloration) and associated foam lines. The photo was taken from an altitude of ~300 m on 6 October in the region of the AUV's southeastern transect. The distance between foam lines was ~100 m.

convergence zones is a visible description of the same physical–biological interactions that may result in the accumulation of motile larvae.

Bloom observations indicate the presence of convergence at multiple scales. The largest scale was that of the entire bloom domain, reaching ~100 km^2 (Fig. 5). During the upwelling response, the bloom was most highly concentrated near the coast (Fig. 5B, C), suggesting accumulation in a convergence zone that formed along the coastal boundary due to shoreward flow of the upwelling filament (Fig. 2C–E). Consistent with this interpretation, the surface drifter showed net shoreward transport, passing closer to the coast with successive diurnal oscillations (Fig. 5C). Smaller scale convergence zones were indicated by filamentous accumulations of phytoplankton. Satellite data revealed finger-like accumulations on scales of ~1 km wide × 3 km long extending into the AUV survey domain (Fig. 5B, C). At yet finer scales, aerial photography revealed parallel bands of reddish water and associated surface foam lines marking the bands' offshore boundary (Fig. 5D). The cross-band separation of foam lines was ~100 m. Convergence indicated at multiple scales was likely an important influence on larval distributions, not only by accumulation of larvae through behavioral–physical interactions, but also through influencing food concentrations.

3.4. Water-column structure, variability and inferred processes

The high spatial and temporal resolutions of the AUV transect series support examination of processes relevant to larval abundance distributions. Physical–biological interactions of the phytoplankton can be evaluated using optical measurements made by the AUV and used to interpret larval distribution data collected at much lower resolution than the optical measurements. The southeastern transect was best positioned for examination of frontal dynamics, and it was most consistently and densely sampled (Sections 3.1 and 3.2). Three variables effectively support this examination (Fig. 6). Temperature represents water types and their frontal boundary, and the combination of chlorophyll fluorescence and optical backscattering represents the distributions of particles subject to transport. Variation in water column structure is examined relative to regional tidal and sea breeze forcing (Fig. 6, top panel) and water column velocity at the southern end of the AUV transect (Fig. 7).

Cooling of the upper water column caused by the upwelling response (Figs. 2, 3) is pronounced in the AUV section series (Fig. 6A–C). While the temperature range in the water column remained relatively

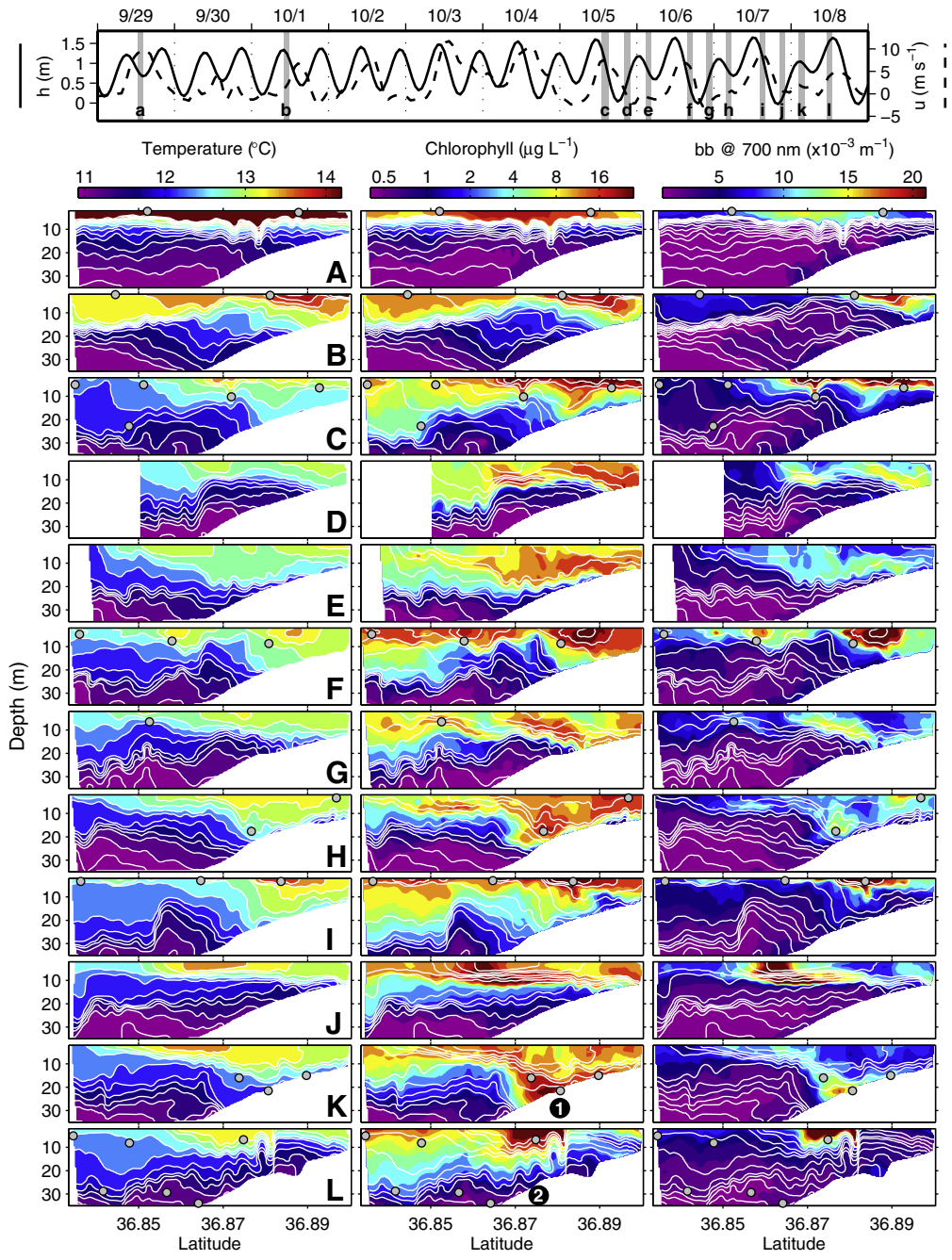

Fig. 6. Water column time-series for the southeastern AUV transect. The top panel shows transect observation times (shaded) relative to surface tidal height (h) at Moss Landing and zonal wind (u) along the northern coast (sampling locations shown in Fig. 1). Zonal wind at this location represents the sea breeze that strongly affects the Monterey Bay upwelling shadow (Woodson et al., 2009). Each AUV transect is interpolated from up to 70 profiles (for full transect coverage) sampled in 1.5–2.1 hours. Temperature contours are overlaid in chlorophyll and optical backscattering panels. The locations of autonomously triggered water samples are indicated by gray circles. Labels 1 and 2 (in chlorophyll transects K and L) identify locations where the two highest larval concentrations encountered in this study were sampled.

constant during the intensive observations of 5–8 October, the spatial distribution of warm near-surface water relative to the underlying cooler water varied dramatically (Fig. 6C–L). The water velocity profile at the southern end of the transect shows influence of vertical shear, which was more prevalent in the cross-shore component (Fig. 7A) than in the along-shore component (Fig. 7B). The first set of transects observed during consecutive falling-rising-falling tidal phases was sampled on 5–6 October (Fig. 6 top, transects c–e). During the rising tide, cold (<12 °C) deep-shelf water was closer to the coast (Fig. 6D), relative to the adjacent falling tidal phases (Fig. 6C, E). Shoreward movement of the cold deep-shelf water followed a period of onshore transport (Fig. 7A, shaded contours below 20 m during and following transect C). Differential displacement of warm near-surface water and underlying cold water was similarly evident in subsequent cycles of tidal variation (Fig. 6F–H, I–K), consistent with the vertically sheared flow (Fig. 7A). Velocity shear over the shelf may have been forced by tidal motions (Baines, 1982) and/or inertial motions associated with the diurnal winds (Simpson et al., 2002). Because of the similar periodicity and timing of tidal and wind forcing during our study (Fig. 6, top panel) and the relatively short period of this study, it is not possible to isolate shear forcing mechanisms.

Associated with the strongly sheared flow, the synoptic structure of the water column indicated convergence and associated vertical circulation in the frontal zone. During the initial falling tide of the first

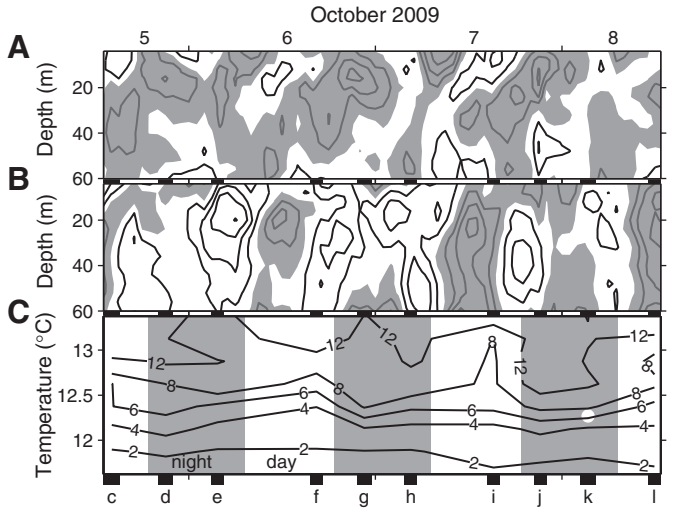

Fig. 7. Circulation and plankton vertical migration. (A) Cross-shelf, and (B) along-shelf velocity at mooring M0, the southern limit of the AUV transects shown in Fig. 6; positive values are within the shaded contours; contour interval is 5 cm s^{-1}. (C) Average chlorophyll concentrations within temperature-range bins of each AUV transect (Fig. 6); nighttime periods are shaded. The white circle during the night of 8 October indicates the temperature of the near-bottom chlorophyll patch within which the highest larval concentrations were detected (Figs. 4, 6K). Letters along the bottom of panel C correspond with the section identifications shown in the top panel of Fig. 6.

well-sampled tidal cycle, a filament of phytoplankton-enriched water, evident in both chlorophyll fluorescence and optical backscattering, extended from the surface layer downward to nearly the seafloor (between ~36.88 and 36.89°N in Fig. 6C). At that time, cross-shelf flow was offshore in the upper 20 m and onshore below (Fig. 7A). We interpret that convergence developed between the shoreward flowing cold water, which was shoaling along the bathymetry, and the overlying warm surface layer (Fig. 6C), and that the associated downwelling transported phytoplankton downward from the surface layer. Following further shoreward progression of the cold deep-shelf water, a phytoplankton biomass maximum extended from surface to bottom along the shoreward face of the cold intrusion (Fig. 6D). These observations suggest physical control over the distributions of phytoplankton through downwelling in the convergence zone and shoreward advection with the cold intrusion.

While vertical transport of phytoplankton by physical processes is indicated, biological influence is also evident. Phytoplankton distributions exhibited a diurnal cycle consistent with light–modulated swimming behavior. The AUV transects show accumulation of phytoplankton near the surface during the day (Fig. 6, chlorophyll panels C, F, I, and L) and formation of subsurface maxima during the dark hours of night to early morning (Fig. 6, chlorophyll panels D, E, G, H, J and K). This apparent vertical migration is supported by the quasi-diurnal vertical displacement of chlorophyll fluorescence signal relative to temperature (Fig. 7C), which more clearly isolates vertical displacement that may be due to behavior. These patterns are consistent with the behavior of dinoflagellates (Fig. 5), which swim to near-surface water during the day for photosynthesis and down to the thermocline/nutricline at night for nutrient acquisition (Smayda, 1997). This behavior has been documented in studies of Monterey Bay and related to dense accumulations of cells at the surface and within the water column at the nutricline (Ryan et al., 2009, 2010b; Sullivan et al., 2010). The leading face of the cold intrusion was a nutricline (nitrate data not shown), thus behavior may have also played a role in the repeated formation of a phytoplankton abundance maximum along the leading face of the cold intrusion (Fig. 6D, G, J, K).

3.5. Case studies of high larval concentrations

The maximum concentrations of both mussel and barnacle larvae sampled in the entire study were found in a phytoplankton patch along the shoreward face of the cold deep-shelf water, the only time that a phytoplankton maximum in a transect was found adjacent to the seafloor (label 1 in Fig. 6K). This sample is also distinguished as having the highest chlorophyll concentrations of any sample acquired in its temperature range throughout the study (Fig. 4C). The sample was acquired when upwelling frontal gradients were the strongest of the time-series (8 October in Fig. 3), which may imply stronger circulation anomalies associated with frontal dynamics. We hypothesize that the coincidence of high concentrations of phytoplankton and larvae adjacent to the seafloor resulted from accumulation through the interaction of planktonic swimming behavior and downwelling in a frontal convergence zone (Section 3.4), which may have occurred prior to and/or during subduction to the bottom.

Although behavior may explain some of the subsurface accumulation of phytoplankton (Section 3.4), it cannot fully explain the anomalous attributes of the phytoplankton patch within which the highest larval concentrations were detected. Vertical migration of the phytoplankton was constrained to temperatures greater than ~12.5 °C (Figs. 6, 7C), whereas the phytoplankton patch containing the highest larval concentrations was sampled in colder water (Fig. 6K). The white circle in Fig. 7C during the night of 7–8 October emphasizes the location of this high chlorophyll patch below the temperature range of phytoplankton diurnal vertical migration. These observations support the conclusion that beyond behavior, downwelling in convergent frontal circulation (Section 3.4) subducted phytoplankton, and presumably larvae, to the bottom. In this dynamic frontal zone, autonomously targeted sampling yielded detection of the highest larval concentrations in our study within a phytoplankton patch located where we would not have predicted it to be – adjacent to the seafloor.

Previous studies have interpreted larval accumulation in fronts. A conceptual model based on studies of intertidal barnacle recruitment in the Monterey Bay region suggests that during upwelling larvae accumulate in fronts where upwelled water interfaces with offshore water, and during relaxation of upwelling recruitment pulses result from transport of front-accumulated larval populations to the coast (Farrell et al., 1991; Roughgarden et al., 1991). Wing et al. (1998) describe crab and rockfish larvae being concentrated in an upwelling front in the Gulf of the Farallones. Shanks et al. (2000) show that relaxing upwelling fronts off the U.S. east coast may concentrate larvae and transport them toward the coast. Accumulation of bivalve and gastropod larvae is likewise known for convergent estuarine plume fronts in Chesapeake Bay (Shanks et al., 2002). Intensive study of Monterey Bay yielded a conceptual model in which accumulation of larvae results from the interaction between flow convergence in the upwelling shadow front and larval behavior, and enhanced recruitment results from along-front transport of accumulated larvae toward the coast (Woodson et al., 2009). This model is supported by examination of frontal locations defined by remote sensing data and recruitment data from intertidal and nearshore reef habitats (Woodson et al., 2012).

The second highest larval concentrations of the entire study were also sampled late in the experiment, when frontal gradients were at a maximum (Fig. 3). The label 2 in Fig. 6L is located directly below this sample, which was acquired within a dense phytoplankton patch near the surface. In addition to a shallow thermal front at the seaward boundary of the upwelling shadow (near 36.86°N), a sharper thermal front was present within the upwelling shadow near 36.88°N, at the shoreward end of the warm, chlorophyll-enriched patch that was sampled. The sharpness of this frontal boundary was linked to internal wave (IW) perturbation of isotherms, and the distribution of warm, phytoplankton-rich surface water was modified by the IWs. The multiple crests and troughs between 36.87°N and 36.88°N, decreasing in amplitude with increasing water depth, indicate an IW packet.

Assuming that the deepest IW trough toward the northern (inshore) side was leading the wave packet, then the water sampled by the AUV would have experienced two full wave oscillations (Fig. 6L). For linear waves the effects of convergent wave troughs and divergent wave crests would presumably cancel through two complete wave oscillations. However, the leading wave was nonlinear, which can cause net convergence due to asymmetry in the horizontal velocities and temperature contours across the wave trough, and the potential development of a trapped core of fluid within the wave (Lamb, 1997; Scotti and Pineda, 2004; Shroyer et al., 2010). The nonlinearity of the leading wave is supported by the ratio of the wave amplitude ($a = 8.7$ m) to the surface layer depth ($H = 5.6$ m): $a/H > 1$ (Barad and Fringer, 2010; Bogucki and Garrett, 1993). Based on this criterion the trailing waves in the packet appear to have been linear ($a/H < 1$).

Although no aerial photography coincided directly with these in situ AUV observations, the influence of internal wave convergence on the accumulation of motile phytoplankton in this area was clearly evident in a photograph from two days earlier (Fig. 5D), with implications for the accumulation of motile larvae. Larval accumulation and transport by internal waves have been observed directly (Pineda, 1991; Shanks, 1983; Shanks and Wright, 1987). Additionally, internal wave influence has been inferred from observed relationships between tidal amplitude and larval settlement and recruitment. Shanks (2009) reports that highly pulsed variation in larval barnacle settlement in Oregon coastal waters can be largely explained by variation in tidal amplitude, while much smaller settlement pulses are associated with the onset of upwelling. From a 5-year study in Bodega Bay, Morgan et al. (2009) show that recruitment in 7 out of 8 invertebrate taxa was intermittently correlated with maximum tidal range.

In considering the relative importance of physical and biological forcing of larval distributions, relative variation of different larval species is relevant. For example, very different patterns of abundance between different species may indicate that biological factors such as spawning behavior and motility, and their interaction with environmental variability, dominate control over larval distribution patterns. Strong covariation in the abundance of barnacle and mussel larvae in this study is suggested by representation of their abundances in temporal, spatial and ecological contexts (Fig. 4), and this is more directly evident in a sample-to-sample comparison (Fig. 8). This suggests the dominance of physical processes in controlling the distribution patterns of these two larval taxa during our study.

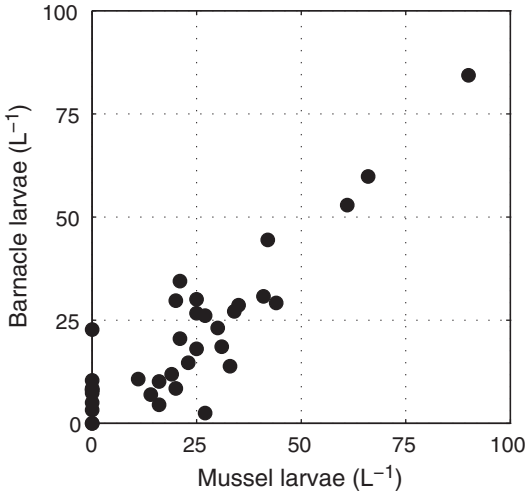

Fig. 8. Sample-to-sample comparison of mussel and barnacle larval abundances.

4. Conclusions

Forced by a spectrum of interacting environmental and biological processes that span a great range of spatial and temporal scales, plankton ecology is complex. By integrating multiscale, multidisciplinary observations, we can augment detection of key processes driving plankton ecology. In this study, observations from satellites, moorings, drifters and an AUV specifically developed for plankton research were integrated to examine phytoplankton and larval distributions and to infer processes. Observations of phytoplankton distributions were relevant to inferring processes driving larval distributions for two reasons. First, processes evident in the relationships between environmental variability and the distributions of motile phytoplankton have implications for understanding the distributions of motile larvae. Second, unlike larvae, phytoplankton distributions can be described with remote and in situ optical sensing. Retention of near-surface water and plankton within the upwelling shadow was evident in satellite and drifter observations. Formation of a convergence zone between inflowing upwelled water and the coast was indicated by the spatial distribution of a phytoplankton bloom and the drifter trajectory. Accumulation of motile phytoplankton within this ~100 km^2 area represented the largest scale at which behavioral–physical interactions may have resulted in planktonic accumulation. At smaller scales, both remote sensing and in situ observations indicated convergence driven by frontal and internal wave dynamics, and associated accumulations of phytoplankton and larvae. By simultaneously influencing the distributions of phytoplankton and larvae, it is probable that convergence at multiple scales also influenced the nutritional environment of the larvae.

Acknowledgments

This research was supported by the David and Lucile Packard Foundation. Molecular analyses of AUV-acquired water samples were supported by the lab of R. Vrijenhoek (MBARI). We thank R. Vrijenhoek for helpful discussion and advice on the content of this manuscript. M0 mooring data were provided by the Center for Integrated Marine Technology under NOAA award NA160C2936. R. McEwen and J. Bellingham contributed to the development of the Dorado AUV's phytoplankton patch sampling algorithms. We thank the Dorado AUV team: H. Thomas, D. Thompson and D. Conlin, and R/V Zephyr crew for support of AUV operations. Drifter deployments were supported by the NSF Marine Advanced Technology Education program, through the efforts of A. Hochstaedter and students of Monterey Peninsula College. MERIS data were provided by the European Space Agency and processed by D. Foley of the NOAA Coastwatch Program. MODIS Level 1 data were provided by the NASA Level 1 and Atmosphere Archive and Distribution System (LAADS), and MODIS data processing was enabled by the NASA MODIS Ocean Biology Processing Group and the NASA SeaDAS software development team. **[SS]**

References

Baines, P.G., 1982. On internal tide generation models. Deep Sea Res. A 29, 307–338.
Barad, M.F., Fringer, O.B., 2010. Simulations of shear instabilities in interfacial gravity waves. J. Fluid Mech. 644, 61–95.
Barber, R.T., Smith, R.L., 1981. Coastal upwelling ecosystems. In: Longhurst, A.R. (Ed.), Analysis of marine ecosystems. Academic Press, London, pp. 31–68.
Bellingham, J.G., Streitlien, K., Overland, J., Rajan, S., Stein, P., Stannard, J., Kirkwood, W., Yoerger, D., 2000. An Arctic basin observational capability using AUVs. Oceanography 13, 64–71.
Bird, L.E., Sherman, A.D., Ryan, J.P., 2007. Development of an active, large volume, discrete seawater sampler for autonomous underwater vehicles. Proc. Oceans MTS/IEEE, Vancouver, Canada.
Bogucki, D., Garrett, C., 1993. A simple model for the shear-induced decay of an internal solitary wave. J. Phys. Oceanogr. 23, 1767–1776.
Breaker, L.C., Broenkow, W.W., 1994. The circulation of Monterey Bay and related processes. Oceanogr. Mar. Biol. Annu. Rev. 32, 1–64.
Carson, H.S., 2010. Population connectivity of the Olympia oyster in southern California. Limnol. Oceanogr. 55, 134–148.

Cazenave, F., Zhang, Y., McPhee-Shaw, E., Bellingham, J.G., Stanton, T.P., 2011. High-resolution surveys of internal tidal waves in Monterey Bay, California, using an autonomous underwater vehicle. Limnol. Oceanogr. Methods 9, 571–581.
Cowen, R.K., Paris, C.B., Srinivasan, A., 2006. Scaling of connectivity in marine populations. Science 311 (5760), 522–527.
Cullen, J.J., Eppley, R.W., 1981. Chlorophyll maximum layers of the Southern California Bight and possible mechanisms of their formation and maintenance. Oceanol. Acta 4, 23–32.
Davoren, G.K., May, C., Penton, P., Reinfort, B., Buren, A., Burke, C., Andrews, D., Montevecchi, W.A., Record, N., Young, B., et al., 2007. An ecosystem-based research program for capelin (*Mallotus villosus*) in the northwest Atlantic: overview and results. J. Northwest Atl. Fish. Sci. 39, 35–48.
Farrell, T.M., Bracher, D., Roughgarden, J., 1991. Cross-shelf transport causes recruitment to intertidal populations in central California. Limnol. Oceanogr. 36, 279–288.
Fenberg, P.B., Caselle, J.E., Claudet, J., Clemence, M., Gaines, S.D., Garcia-Charton, J.A., Goncalves, E.J., Grorud-Colvert, K., Guidetti, P., Jenkins, S.R., et al., 2012. The science of European marine reserves: status, efficacy, and future needs. Mar. Policy 36, 1012–1021.
Fitzwater, S.E., Johnson, K.S., Elrod, V.A., Ryan, J.P., Coletti, L.J., Tanner, S.J., Gordon, R.M., Chavez, F.P., 2003. Iron, nutrient and phytoplankton biomass relationships in upwelled waters of the California coastal system. Cont. Shelf Res. 23, 1523–1544.
Franks, P.J.S., 1997. Spatial patterns in dense algal blooms. Limnol. Oceanogr. 42, 1297–1305.
Gaines, S.D., White, C., Carr, M.H., Palumbi, S.R., 2010. Designing marine reserve networks for both conservation and fisheries management. Proc. Natl. Acad. Sci. 107, 18286–18293.
Goffredi, S.K., Jones, W.J., Scholin, C.A., Marin III, R., Vrijenhoek, R.C., 2006. Molecular detection of marine invertebrate larvae. Mar. Biotechnol. 8, 149–160.
Gower, J., King, S., Borstad, G., Brown, L., 2005. Detection of intense plankton blooms using the 709 nm band of the MERIS imaging spectrometer. Int. J. Remote Sens. 26, 2005–2012.
Graham, W.M., Largier, J.L., 1997. Upwelling shadows as nearshore retention sites: the example of northern Monterey Bay. Cont. Shelf Res. 17, 509–532.
Graham, W.M., Field, J.G., Potts, D.C., 1992. Persistent 'upwelling shadows' and their influence on zooplankton distributions. Mar. Biol. 114, 561–570.
Harvey, J.B.J., Ryan, J.P., Marin III, R., Preston, C.M., Alvarado, N., Scholin, C.A., Vrijenhoek, R. C., 2012. Robotic sampling, in situ monitoring and molecular detection of marine zooplankton. J. Exp. Mar. Biol. Ecol. 413, 60–70.
Harvey, J.B.J., Djunaedi, A.F., Vrijenhoek, R.C., 2013. Validation of a sandwich hybridization assay for marine copepod detection. J. Exp. Mar. Biol. Ecol. 446, 306–310.
Holm-Hansen, O., Amos, A.F., Hewes, C.D., 2000. Reliability of estimating chlorophyll a concentrations in Antarctic waters by measurement of in situ chlorophyll a fluorescence. Mar. Ecol. Prog. Ser. 196, 103–110.
Johnson, K.S., Needoba, J.A., 2008. Mapping the spatial variability of plankton metabolism using nitrate and oxygen sensors on an autonomous underwater vehicle. Limnol. Oceanogr. 53, 2237–2250.
Jones, W.J., Preston, C.M., Marin III, R., Scholin, C.A., Vrijenhoek, R.C., 2008. A robotic molecular method for in situ detection of marine invertebrate larvae. Mol. Ecol. Resour. 8, 540–550.
Lamb, K.G., 1997. Particle transport by nonbreaking, solitary internal waves. J. Geophys. Res. 102, 18641–18660.
Mace, A.J., Morgan, S.G., 2006. Larval accumulation in the lee of a small headland: implications for the design of marine reserves. Mar. Ecol. Prog. Ser. 318, 19–29.
Manning, J.P., McGillicuddy, D.J., Pettigrew, N., Churchill, J.H., Incze, L.S., 2009. Drifter observations of the Gulf of Maine coastal current. Cont. Shelf Res. 29, 835–845.
Morgan, S.G., Fisher, J.L., Mace, A.J., 2009. Larval recruitment in a region of strong, persistent upwelling and recruitment limitation. Mar. Ecol. Prog. Ser. 394, 79–99.
Morgan, S.G., Fisher, J.L., Largier, J.L., 2011. Larval retention, entrainment, and accumulation in the lee of a small headland: recruitment hot spots along windy coasts. Limnol. Oceanogr. 56, 161–178.
Palumbi, S.R., 2003. Population genetics, demographic connectivity, and the design of marine reserves. Ecol. Appl. 13, S146–S158.
Pineda, J., 1991. Predictable upwelling and the shoreward transport of planktonic larvae by internal tidal bores. Science 253, 548–551.
Rosenfeld, L.K., Schwing, F.B., Garfield, N., Tracy, D.E., 1994. Bifurcated flow from an upwelling center: a cold water source for Monterey Bay. Cont. Shelf Res. 14, 931–964.
Roughan, M., Mace, A.J., Largier, J.L., Morgan, S.G., Fisher, J.L., Carter, M.L., 2005. Subsurface recirculation and larval retention in the lee of a small headland: a variation on the upwelling shadow theme. J. Geophys. Res. C 110, C10027. http://dx.doi.org/10.1029/2005JC002898.
Roughgarden, J., Pennington, J.T., Stoner, D., Alexander, S., Miller, K., 1991. Collisions of upwelling fronts with the intertidal zone: the cause of recruitment pulses in barnacle populations of central California. Acta Ecol. 12, 35–51.
Ryan, J.P., Gower, J.F.R., King, S.A., Bissett, W.P., Fischer, A.M., Kudela, R.M., Kolber, Z., Mazzillo, F., Rienecker, E.V., Chavez, F.P., 2008. A coastal ocean extreme bloom incubator. Geophys. Res. Lett. 35, L12602. http://dx.doi.org/10.1029/2008GL034081.
Ryan, J.P., Fischer, A.M., Kudela, R.M., Gower, J.F.R., King, S.A., Marin III, R., Chavez, F.P., 2009. Influences of upwelling and downwelling winds on red tide bloom dynamics in Monterey Bay, California. Cont. Shelf Res. 29, 785–795.
Ryan, J.P., Johnson, S.B., Sherman, A., Rajan, K., Py, F., Thomas, H., Harvey, J.B.J., Bird, L., Paduan, J.D., Vrijenhoek, R.C., 2010a. Mobile autonomous process sampling within coastal ocean observing systems. Limnol. Oceanogr. Methods 8, 394–402.
Ryan, J.P., McManus, M.A., Sullivan, J.M., 2010b. Interacting physical, chemical and biological forcing of phytoplankton thin-layer variability in Monterey Bay, California. Cont. Shelf Res. 30, 7–16.
Ryan, J.P., Fischer, A.M., Kudela, R.M., McManus, M.A., Myers, J.S., Paduan, J.D., Ruhsam, C. M., Woodson, C.B., Zhang, Y., 2010c. Recurrent frontal slicks of a coastal ocean upwelling shadow. J. Geophys. Res. C 115, C12070. http://dx.doi.org/10.1029/2010JC006398.
Ryan, J.P., Greenfield, D., Marin III, R., Preston, C., Roman, B., Jensen, S., Pargett, D., Birch, J., Mikulski, C., Doucette, G., Scholin, C., 2011. Harmful phytoplankton ecology studies using an autonomous molecular analytical and ocean observing network. Limnol. Oceanogr. 56, 1255–1272.
Ryan, J.P., McManus, M.A., Kudela, R.M., Lara Artigas, M., Bellingham, J.G., Chavez, F.P., Doucette, G., Foley, D., Godin, M., Harvey, J.B.J., Marin III, R., Messié, M., Mikulski, C., Pennington, T., Py, F., Rajan, K., Shulman, I., Wang, Z., Zhang, Y., 2014. Boundary influences on HAB phytoplankton ecology in a stratification-enhanced upwelling shadow. Deep-Sea Res. II 101, 63–79. http://dx.doi.org/10.1016/j.dsr2.2013.01.017.
Ryther, J.H., 1955. Ecology of autotrophic marine dinoflagellates with reference to red water conditions. In: Johnson, F.H. (Ed.), The Luminescence of Biological Systems. American Association for the Advancement of Science, pp. 387–414.
Scotti, A., Pineda, J., 2004. Observation of very large and steep internal waves of elevation near the Massachusetts coast. Geophys. Res. Lett. 31, L22307. http://dx.doi.org/10.1029/2004GL021052.
Shanks, A.L., 1983. Surface slicks associated with tidally forced internal waves may transport pelagic larvae of benthic invertebrates and fishes shoreward. Mar. Ecol. Prog. Ser. 13, 311–315.
Shanks, A.L., 2009. Barnacle settlement versus recruitment as indicators of larval delivery. II. Time-series analysis and hypothesized delivery mechanisms. Mar. Ecol. Prog. Ser. 385, 217–226.
Shanks, A.L., Wright, W.G., 1987. Internal-wave-mediated shoreward transport of cyprids, megalopae, and gammarids and correlated longshore differences in the settling rate of intertidal barnacles. J. Exp. Mar. Biol. Ecol. 114, 1–13.
Shanks, A.L., Largier, J., Brink, L., Brubaker, J., Hooff, R., 2000. Demonstration of the onshore transport of larval invertebrates by the shoreward movement of an upwelling front. Limnol. Oceanogr. 45, 230–236.
Shanks, A.L., Largier, J., Brink, L., Brubaker, J., Hooff, R., 2002. Observations on the distribution of meroplankton during a downwelling event and associated intrusion of the Chesapeake Bay estuarine plume. J. Plankton Res. 24, 391–416.
Shroyer, E.L., Moum, J.N., Nash, J.D., 2010. Vertical heat flux and lateral mass transport in nonlinear internal waves. Geophys. Res. Lett. 37, L08601. http://dx.doi.org/10.1029/2010GL042715.
Simpson, J.H., Hyder, P., Rippeth, T.P., Lucas, I.M., 2002. Forced oscillations near the critical latitude for diurnal-inertial resonance. J. Phys. Oceanogr. 32, 177–187.
Smayda, T.J., 1997. Harmful algal blooms: their ecophysiology and general relevance to phytoplankton blooms in the sea. Limnol. Oceanogr. 42, 1137–1153.
Sponaugle, S., 2009. Otolith microstructure reveals ecological and oceanographic processes important to ecosystem-based management. Environ. Biol. Fish 86, 221–238.
Stumpf, R.P., Litaker, R.W., Lanerolle, L., Tester, P.A., 2008. Hydrodynamic accumulation of *Karenia* off the west coast of Florida. Cont. Shelf Res. 28, 189–213.
Sullivan, J.M., Donaghay, P.L., Rines, J.E.B., 2010. Coastal thin layer dynamics: consequences to biology and optics. Cont. Shelf Res. 30, 50–65.
Wing, S.R., Botsford, L.W., Ralston, S.V., Largier, J.L., 1998. Meroplanktonic distribution and circulation in a coastal retention zone of the northern California upwelling system. Limnol. Oceanogr. 43, 1710–1721.
Wing, S.R., Botsford, L.W., Morgan, L.E., Diehl, J.M., Lundquist, C.J., 2003. Inter-annual variability in larval supply to populations of three invertebrate taxa in the northern California current. Estuar. Coast. Shelf Sci. 57, 859–872.
Woodson, C.B., Washburn, L., Barth, J.A., Hoover, D.J., Kirincich, A.R., McManus, M.A., Ryan, J.P., Tyburczy, J., 2009. The northern Monterey Bay upwelling shadow front: observations of a coastally- and surface-trapped buoyant plume. J. Geophys. Res. 114, C12013. http://dx.doi.org/10.1029/2009JC005623.
Woodson, C.B., McManus, M.A., Tyburczy, J.A., Barth, J.A., Washburn, L., Caselle, J.E., Carr, M.H., Malone, D.P., Raimondi, P.T., Menge, B.A., Palumbi, S.R., 2012. Coastal fronts set recruitment and connectivity patterns across multiple taxa. Limnol. Oceanogr. 57, 582–596.
Zhang, Y., McEwen, R.S., Ryan, J.P., Bellingham, J.G., 2010. Design and tests of an adaptive triggering method for capturing peak samples in a thin phytoplankton layer by an autonomous underwater vehicle. IEEE J. Ocean. Eng. 35, 785–796.
Zhang, Y., Ryan, J.P., Bellingham, J.G., Harvey, J.B.J., McEwen, R.S., 2012. Autonomous detection and sampling of water types and fronts in a coastal upwelling system by an autonomous underwater vehicle. Limnol. Oceanogr. Methods 10, 934–951.